# High dynamic range coherent imaging using compressed sensing

**Kuan He,* Manoj Kumar Sharma and Oliver Cossairt**

*Department of Electrical Engineering and Computer Science, Northwestern University, Evanston, IL, 60208, USA*
*hekuan@u.northwestern.edu

**Abstract:** In both lensless Fourier transform holography (FTH) and coherent diffraction imaging (CDI), a beamstop is used to block strong intensities which exceed the limited dynamic range of the sensor, causing a loss in low-frequency information, making high quality reconstructions difficult or even impossible. In this paper, we show that an image can be recovered from high-frequencies alone, thereby overcoming the beamstop problem in both FTH and CDI. The only requirement is that the object is sparse in a known basis, a common property of most natural and manmade signals. The reconstruction method relies on compressed sensing (CS) techniques, which ensure signal recovery from incomplete measurements. Specifically, in FTH, we perform compressed sensing (CS) reconstruction of captured holograms and show that this method is applicable not only to standard FTH, but also multiple or extended reference FTH. For CDI, we propose a new phase retrieval procedure, which combines Fienup's hybrid input-output (HIO) method and CS. Both numerical simulations and proof-of-principle experiments are shown to demonstrate the effectiveness and robustness of the proposed CS-based reconstructions in dealing with missing data in both FTH and CDI.



**OCIS codes:** (110.1650) Coherence imaging; (100.5070) Phase retrieval; (110.3010) Image reconstruction techniques; (090.1995) Digital holography; (050.1940) Diffraction.

## References and links

1. J. M. Zuo, I. Vartanyants, M. Gao, R. Zhang, and L. A. Nagahara, "Atomic resolution imaging of a carbon nanotube from diffraction intensities," Science **300**(5624), 1419-1421 (2003).
2. P. Thibault, V. Elser, C. Jacobsen, D. Shapiro, and D. Sayre, "Reconstruction of a yeast cell from X-ray diffraction data," Acta Crystallographica Section A, **62**(4) 248–261 (2006).
3. D. Shapiro, P. Thibault, T. Beetz, V. Elser, M. Howells, C. Jacobsen, J. Kirz, E. Lima, H. Miao, A. M. Neiman, and D. Sayre, "Biological imaging by soft x-ray diffraction microscopy," Proceedings of the National Academy of Sciences of the United States of America, **102**(43) 15343–15346 (2005).
4. G. W. Stroke, "Lensless Fourier-transform method for optical holography," Appl. Phys. Lett. **6**(10), 201-203 (1965).
5. I. McNulty, J. Kirz, C. Jacobsen, E. H. Anderson, M. R. Howells, and D. P. Kern, "High-resolution imaging by Fourier transform X-ray holograph," Sciences, **256**, 1009-1012 (1992).
6. S. Eisebitt, J. Lüning, W. F. Schlotter, M. Lörgen, O. Hellwig, W. Eberhardt and J. Stöhr, "Lensless imaging of magnetic nanostructures by x-ray spectro-holography," Nature. **432,** 885-888 (2004).
7. S. Marchesini, S. Boutet, A. E. Sakdinawat, M. J. Bogan, S. Bajt, A. Barty, H. N. Chapman, M. Frank, S. P. Hau-Riege, A. Szöke, C. Cui, D. A. Shapiro, M. R. Howells, J. C. H. Spence, J. W. Shaevitz, J. Y. Lee, J. Hajdu and M. M. Seibert, "Massively parallel x-ray holography," Nat. Photonics **2**, 560-563 (2008).
8. J. R. Fienup, "Phase retrieval algorithms: a comparison," Appl. Opt. **21**, 2758-2769 (1982).
9. J. R. Fienup, "Reconstruction of a complex-valued object from the modulus of its Fourier transform using a support constraint," J. Opt. Soc. Am. A **4**, 118-123 (1987).
10. J. N. Cederquist, J. R. Fienup, J. C. Marron, and R. G. Paxman, "Phase retrieval from experimental far-field speckle data." Opt. Lett. **13**, 619-621 (1988).
11. J. Miao, P. Charalambous, J. Kirz and D. Sayre, "Extending the methodology of X-ray crystallography to allow imaging of micrometre-sized non-crystalline specimens," Nature **400,** 342–344 (1999).
12. S. Marchesini, H. He, H. N. Chapman, S. P. Hau-Riege, A. Noy, M. R. Howells, U. Weierstall and J. C. H. Spence, "X-ray image reconstruction from a diffraction pattern alone," Phys. Rev. B **68,** 140101 (2003).

13. H. N. Chapman, A. Barty, S. Marchesini, A. Noy, S. P. Hau-Riege, C. Cui, M. R. Howells, R. Rosen, Haifeng He, John C. H. Spence, U. Weierstall, T. Beetz, C. Jacobsen and D. Shapiro, "High-resolution *ab initio* three-dimensional x-ray diffraction microscopy," J. Opt. Soc. Am. A **23,** 1179–1200 (2006).
14. W. F. Schlotter, R. Rick, K. Chen, A. Scherz, J. Stöhr, J. Löning, S. Eisebitt, Ch. Günther, W. Eberhardt, O. Hellwig and I. McNulty, "Multiple reference Fourier transform holography with soft x rays," Appl. Phys. Lett. **89**, 163112 (2006).
15. M. Giozar-Sicairos and J. R. Fienup, "Holography with extended reference by autocorrelation linear differential operation," Opt. Express **15**, 17592–17612 (2007).
16. M. Giozar-Sicairos and J. R. Fienup, "Direct image reconstruction from a Fourier intensity pattern using HERALDO," Opt. Lett. **33**, 2668-2670 (2008).
17. D. Gauthier, M. Giozar-Sicairos, X. Ge, W. Boutu, B. Carré, J. R. Fienup, and H. Merdji. "Single-shot femtosecond x-ray holography using extended references." Phys. Rev. Lett. **105**, 093901 (2010).
18. J. Miao, T. Ishikawa, E. H. Anderson and K. O. Hodgson, "Phase retrieval of diffraction patterns from noncrystalline samples using the oversampling method." Phys. Rev. B **67**(17), 174104 (2003).
19. J. Miao, Y. Nishino, Y. Kohmura, B. Johnson, C. Song, S. H. Risbud and T. Ishikawa, "Quantitative image reconstruction of GaN quantum dots from oversampled diffraction intensities alone." Phys. Rev. Lett. **95**, 085503 (2005).
20. X. Huang, J. Nelson, J. Steinbrener, J. Kirz, J. J. Turner and C. Jacobsen, "Incorrect support and missing center tolerances of phasing algorithms," Opt. Express **18**(25), 26441-26449 (2010).
21. R. N. Wilke, M. Vassholz, and T. Salditt, "Semi-transparent central stop in high-resolution X-ray ptychography using Kirkpatrick–Baez focusing," Acta Crystallographica Section A, **69**(5) 490–497 (2013).
22. Y. Nishino, J. Miao, and T. Ishikawa, "Image reconstruction of nanostructured nonperiodic objects only from oversampled hard x-ray diffraction intensities," Phys. Rev. B **68**, 220101 (2003).
23. E. J. Candès, J. Romberg, and T. Tao, "Robust uncertainty principles: exact signal reconstruction from highly incomplete frequency information," IEEE Trans. Inf. Theory **52**, 489–509 (2006).
24. E. J. Candès and T. Tao, "Near-optimal signal recovery from random projections: Universal encoding strategies?" IEEE Trans. Inf. Theory **52**, 5406–5425 (2006).
25. E. J. Candès and M. B.Wakin, "An introduction to compressive sampling," IEEE Signal Process. Mag. **25**, 21–30 (2008).
26. D. L. Donoho, "Compressed sensing," IEEE Trans. Inf. Theory **52**, 1289–1306 (2006).
27. E. J. Candès and J. Romberg, "Sparsity and incoherence in compressive sampling," Inverse Problems, **23**, 969–985 (2007).
28. D. J. Brady, K. Choi, D. L. Marks, R. Horisaki and S. Lim, "Compressive Holography," Opt. express, **17,** 13040-13049 (2009).
29. Y. Rivenson, A. Stern, and B. Javidi, "Compressive Fresnel Holography," J. Display Technol. **6,** 506-509 (2010).
30. L. Michael, D. Donoho, and J. M. Pauly. "Sparse MRI: The application of compressed sensing for rapid MR imaging." Magnetic resonance in medicine **58,** 1182-1195 (2007).
31. S. Gazit, A. Szameit, Y. C. Eldar, and M. Segev, "Super-resolution and reconstruction of sparse sub-wavelength images," Opt. Express, **17,** 23920-23946 (2009).
32. A. Szameit, Y. Shechtman, E. Osherovich, E. Bullkich, P. Sidorenko, H. Dana, S. Steiner, E. B. Kley, S. Gazit, T. Cohen-Hyams, S. Shoham, M. Zibulevsky, I. Yavneh, Y. C. Eldar, O. Cohen and M. Segev, "Sparsity-based single-shot subwavelength coherent diffractive imaging," Nature Materials, **11**, 455-459 (2012).
33. Y. Shechtman, Y. C. Eldar, O. Cohen, H. N. Chapman, M. Jianwei and M. Segev, "Phase retrieval with application to optical imaging," Signal Processing Magazine, IEEE, **32**(3), 87-109 (2015)
34. E. J. Candès, J. Romberg, and T. Tao, "Stable Signal Recovery from Incomplete and Inaccurate Measurements," Comm. Pure and Applied Math., **59**, 1207-1223 (2006).
35. L. I. Rudin, S. Osher, and E. Fatemi, "Nonlinear total variation based noise removal algorithms," Physica D, **60,** 259-268 (1992).
36. E. J. Candès and J. Romberg, "$l_1$-Magic: Recovery of Sparse Signals via Convex Programming," http://www.acm.caltech.edu/l1magic/downloads/l1magic, (2005).
37. F. H. C. Tivive and A. Bouzerdoum. "A compressed sensing method for complex-valued signals with application to through-the-wall radar imaging," in *Pro. IEEE Int. Conf. Acoust. Speech Signal Process. (ICASSP), Vancouver, Canada*, 2144-2148 (2014).

## 1. Introduction

Lensless imaging with coherent X-rays has demonstrated great potential in recent years in the field of biology and material science [1-3]. Instead of forming images directly, the technique captures a far-field diffraction pattern, then recovers an image computationally. However, the method requires phase retrieval because only the intensity of the scattered signal is detected on the sensor. There are two fundamental solutions to the phase retrieval problem: holography and image reconstruction by iterative phase retrieval [8-13]. Accordingly, two lensless imaging modalities have been proposed and are commonly used in experiments: Fourier transform holography [4-7] and Coherent Diffraction Imaging (CDI) using iterative phase retrieval.

FTH is a non-iterative lensless imaging technique in which the phase information of the scattered wave is encoded in the intensity of the diffraction pattern and the desired image is recovered in a single-step deterministic computation [4-6]. This is achieved by introducing a reference wave generated from a point source in the vicinity of the object. The interference between the reference wave and the object wave forms a hologram in the far-field plane of the object. The object is then retrieved by a simple inverse Fourier transform of the recorded hologram. For FTH, the resolution is limited by the size of the reference point source, which is inversely proportional to the reference flux. To improve the resolution while maintaining sufficient reference intensity, various holography schemes have been developed. Examples include multiple reference FTH [14], uniformly redundant arrays (URAs) reference FTH [7], and holography with extended reference by autocorrelation linear differential operation (HERALDO) [15-17].

CDI is another commonly used lensless imaging technique in the X-ray regime. In CDI, the intensity of the diffraction field should be at least Nyquist sampled and phase is recovered iteratively [8, 9]. In these algorithms, at each iteration, constraints are imposed in both Fourier space and real space. The Fourier constraints are the intensity values measured by the detector and the real-space constraints are the object support, which may be known *a priori* or estimated from the object's autocorrelation [12]. In principle, the resolution of reconstructed CDI images depends on the maximum diffraction angle and the illumination wavelength.

A fundamental problem common to both CDI and FTH is the presence of missing data, as shown in Fig. 1. Due to the limited dynamic range of CCDs, a beamstop is often used to block the central region of the diffraction pattern. Since this region corresponds to low-spatial-frequencies in the object, losing this data makes image reconstruction difficult or even impossible [19-22]. Attempts to overcome this problem fall into three categories: (1) replace the missing data with a calculated Fourier modulus of a lower resolution image of the object captured from an x-ray or electron microscope [1, 18]. (2) Design a semi-transparent beam stop [21]. (3) Develop new reconstruction algorithms to address the missing data problem. For example, a modified hybrid input-output (HIO) is proposed in [22] to reconstruct the object with a single intensity measurement.

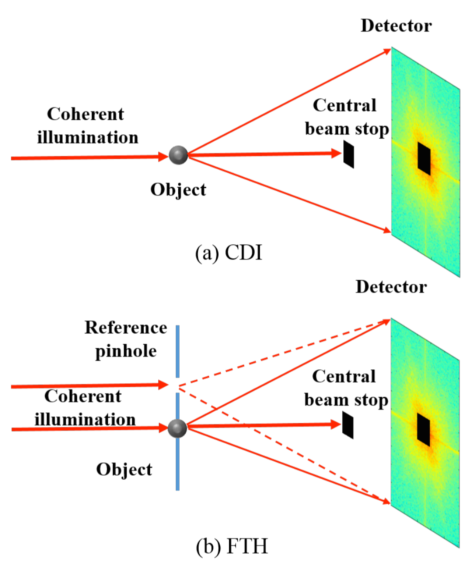


Fig. 1. Beam stop in (a) CDI and (b) FTH, causing central low-frequencies information to be lost in the diffraction pattern.

In this paper, we propose the application of Compressed Sensing (CS) to solve the missing data problem for both FTH and CDI. Our method provides robust phase-retrieval of diffracted fields with large amounts of missing data using just a single measurement. CS [23-27], a recently developed theory, is based on the underlying assumption that the object of interest can be represented sparsely in a suitable basis. CS literature states that such an object can be recovered from an incomplete set of linear measurements [23]. Since its advent, CS has been utilized in a variety of applications to solving missing data problem. For instance, in Fresnel holography, a 3D tomographic reconstruction has been demonstrated from 2D holographic data [28], and 2D images have been reconstructed from incomplete holographic measurements [29]. In magnetic resonance imaging (MRI), an MRI image can be recovered from under-sampled k-space data, significantly reducing acquisition time [30]. Recently, CS has been applied to super-resolution imaging, where high resolution images are recovered from low-frequency information alone [31, 32]. Also, some CS related phase retrieval algorithms [33] have been proposed to solve missing phase problem. In this work, we show that an image can be accurately recovered from high frequencies alone using a CS reconstruction method. The concept is applied directly to both FTH and CDI acquisition schemes, overcoming the missing data problem caused by high-dynamic range diffracted fields. The application to FTH is direct, as the captured hologram is linearly related to the reconstructed image via a Fourier transform. For CDI, the measured diffraction pattern is a nonlinear (quadratic) function of the unknown image. However, we show that the quadratic relationship can be relaxed to be linear if phase is first recovered using Fienup's Hybrid Input-Output (HIO) algorithm [8]. We propose a new technique which combines HIO and CS methods to deal with missing data problem in CDI. We show that the proposed method outperforms the conventional HIO algorithm even when using a large beam stop that produces a significant amount of missing data (i.e. very wide dynamic range diffraction patterns).

## 2. Compressive sensing background

CS theory ensures highly accurate signal reconstruction from far fewer measurements than traditional methods. For simplicity, let us describe CS in one dimension. Let an unknown signal $f$ defined by an $N$-element vector be projected to g, an $M$-element vector. One can think of $g$ as the measurement of $f$. In CS, we are interested in the case of $M<N$, meaning that the number of knowns is less than the number of unknowns. In the case of FTH and CDI where the central data of the diffraction pattern is missing due to the presence of a BS, $N$ is the number of pixels of reconstructed image, $M$ is the number of pixels of diffraction pattern with missing central data, and ($N$-$M$) is the number of missing pixels in the center. The sensing process in CS can be written as (1)

$$g = \Phi f, \tag{1}$$

Where $\Phi$ is an $M \times N$ sensing matrix. Equation (1) is under-determined because the number of unknowns in $f$ is more than the number of measurements in $g$. As a result, the reconstruction of $f$ from Eq. (1) is not unique unless additional information is provided. CS tries to find unique reconstruction by enforcing sparsity constraint on the signal.

We assume that the signal $f$ can be sparsely represented in some arbitrary basis $\Psi$, i.e., wavelets, discrete cosine transform (DCT), or total variation (TV). Thus, the $K$-sparse signal $f$ can be expanded in its sparsity basis $\Psi = (\psi_1 \psi_2 \cdots \psi_N)$ as follows:

$$f = \sum_{i=1}^{N} \alpha_i \cdot \psi_i = \Psi \alpha, \tag{2}$$

where $\alpha = (\alpha_1 \alpha_2 \cdots \alpha_N)^T$ is the coefficient sequence, which has only $K$ nonzero entries and ($N$-$K$) entries that are exactly zeros.

CS theory [23-27] suggests that if $f$ is $K$-sparse in $\Psi$ as shown in Eq. (2), then even with much fewer measurements than traditional methods, an accurate and unique reconstruction from Eq. (1) can be obtained by solving the following $l_1$ minimization problem:

$$\alpha^{\hat{\mathrm{A}}} = \min_{\alpha} \|\alpha\|_{l_1} \text{ subject to } g = \Phi f = \Phi\Psi\alpha, \tag{3a}$$

where $\|\alpha\|_{l_1} = \sum_i |\alpha_i|$ is $l_1$ norm of $\alpha$. Finally, the unknown signal $f$ can be found by multiplying the reconstructed coefficients and the dictionary basis, according to Eq. (2). Essentially, CS seeks a solution with maximum sparsity in the given domain while maintaining fidelity to the measurement. As shown in [34], the CS-based algorithms are able to produce acceptable solutions even with noisy and incomplete measurements. In this case the equality sign in Eq. (3a) becomes inequality, as

$$\alpha^{\hat{\mathrm{A}}} = \min_{\alpha} \|\alpha\|_{l_1} \text{ subject to } \|g - \Phi\Psi\alpha\|_{l_2} \leq \varepsilon, \tag{3b}$$

where $\|\cdot\|_{l_2}$ denotes $l_2$ norm and $\varepsilon$ is the size of the noise in the measurement.

## 3. Image reconstruction from high frequencies only

In this section, we show how a CS approach can help recovering an image from high frequencies alone. The measurement with missing low frequencies can be modeled as

$$O_H = HFo, \tag{1}$$

where $H$ is a high pass filter, $F$ denotes Fourier transform matrix, $o$ is an unknown object, and $O_H$ is high pass filtered frequency spectrum of $o$. Since the low-frequencies are lost in $O_H$ reconstruction of $o$ from $O_H$ is an ill-posed problem. If we inverse Fourier transform Eq. (4), there are an infinite number of solutions possible (i.e., assigning missing low-frequencies with different values while keeping the measured high-frequencies unchanged). Conventionally, an interpolation is often applied to $O_H$ in the Fourier domain. However, it is difficult to estimate the unknown coefficients accurately from nearby Fourier samples alone.

In order to recover the missing low frequency information from $O_H$, additional information must be provided. Here, we exploit knowledge that the image is sparse in some basis and try to reconstruct it using a CS method. Specifically, we enforce the sparsity constraint on the total variation (TV) [35] of $o$, and recover $o$ by solving optimization problem

$$o^{\hat{\mathrm{A}}} = \min_{o} \|o\|_{TV} \text{ subject to } O_H = HFo, \tag{2}$$

where $\|o\|_{TV} = \sum_{n_1} \sum_{n_2} \left| \nabla(o)_{n_1,n_2} \right|$ is TV of $o$. As in Eq. (3b), when noise is present in the measurement, the equality constraint in Eq. (5) changes to an inequality. By solving Eq. (5), we recover the object with minimal complexity (here TV) and also maintain fidelity to the observed data via the constraints on the high frequencies of the reconstruction. Note that Eq. (5) is convex [24, 35] and can be solved efficiently with a generic log-barrier algorithm [36].

This CS technique is demonstrated in the simulation of Fig. 2, showing the ability to recover the unknown signal and its missing low-frequencies in a robust fashion. The original data in Fig. 2(a) represents an image of 256×256 pixels. The spatial frequency spectrum of this image is shown in Fig. 2(b), where the black square marks the cutoff boundaries of the high-pass filter. Here, all the low-frequencies below the cutoff are missing, which is 25% of the total data, concentrated in the center of the Fourier transform. The conventional reconstruction produces a high pass filtered version of the original image [Fig. 2(c)]. With a CS reconstruction, the image is recovered accurately [Fig. 2(d)].

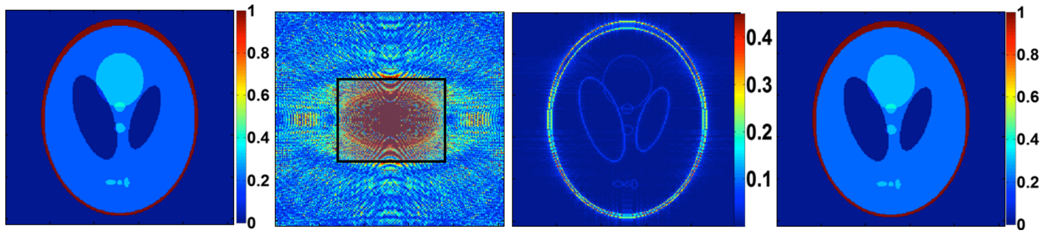


(a) Object (b) FT measurement (c) IFT reconstruction (d) CS reconstruction

Fig. 2. (a) Object, (b) The Fourier spectrum of the object, the black rectangle mimics the beam stop, (c) conventional reconstruction by taking the inverse Fourier transform of the incomplete measurement, (d) CS reconstruction.

## 4. Fourier transform holography (FTH)

### *4.1 Description*

We now show how to apply CS to solve the missing data problem in FTH, due to the presence of a beam stop (BS). In standard FTH [4-6], the exiting wave $f(r)$ after the sample mask consists of the object of interest $o(r)$ and a reference point $\delta(r\text{-}r_0)$, e.g.,

$$f\left(r\right)=o\left(r\right)+\delta\left(r-r_0\right). \tag{3}$$

Then the hologram intensity $I$ can be described as the Fourier transform of the autocorrelation of the function $f(r)$ [5, 6], which is

$$I = FA_{ff}, \tag{4}$$

where $A_{ff}$ is the autocorrelation of $f$, given by

$$A_{ff}\left(r\right)=A_{\delta\delta}\left(r\right)+A_{oo}\left(r\right)+o^*\left(r-r_0\right)+o\left(r+r_0\right). \tag{5}$$

The last term is simply a translated image of the object of interest, and it can be separated from the other three terms provided that the distance $r_0$ between the reference point and the object exceeds the diameter of the object (so-called holographic condition). If we measure the entire hologram, the object image can be reconstructed by a simple inverse Fourier transform. However, in our case, the hologram has a region of missing data due to the presence of a BS. The incomplete measurement can be modeled as

$$I_H = HFA_{ff}, \tag{6}$$

where $H$ is a high-pass filter and $I_H$ denotes the high-pass filtered hologram. Equation (9) is also under-determined and reconstruction of $A_{ff}$ from $I_H$ is an ill-posed problem.

For a conventional holographic reconstruction, we simply perform an inverse Fourier transform on $I_H$. Then Eq. (9) becomes

$$F^{-1}I_H=\left(F^{-1}H\right)*A_{ff}, \tag{7}$$

where $F^{-1}$ is an inverse Fourier transform (IFT) operator and * denotes the convolution. Here, we interpret $F^{-1}H$ as a system point spread function (PSF). Since $H$ is a high pass filter, the intuitive meaning of the PSF is simple: it degrades the image by emphasizing its edges, causing a ringing effect that loses image details (high-pass-effect). By substituting Eq. (8) into Eq. (10), we can clearly see that there are two problems that affect reconstruction quality. First, all four terms in Eq. (8), including the object term, will be degraded by the system PSF. Second, due to the ringing effect, the autocorrelation of the object, which otherwise lies in the center of the reconstruction, may spread over the entire image and therefore, overlap with the object causing the holographic condition to fail.

Using a CS algorithm can ensure accurate image reconstruction from high frequencies alone. By exploiting sparsity in the TV domain, we can reconstruct $A_{ff}$ by solving the following convex problem:

$$\hat{A_{ff}} = \min_{A_{ff}} \left\| A_{ff} \right\|_{TV} \text{ subject to } I_H = HFA_{ff}. \tag{8}$$

Note that according to Eq. (8), $A_{ff}$ contains an image of the autocorrelation of the object $o$, and it can be separated from the other three terms if the holographic condition is met. Again, as shown in Eq. (3b), in the presence of noise, the equality constraint in Eq. (11) changes to an inequality. We remark that although the above derivation is for standard FTH, the results extend to FTH with multiple references [14] or holography with extended reference by autocorrelation linear differential operation (HERALDO) [15-17].

*4.2 Simulation results*

Figures (3) and (4) show numerical simulations for image reconstructions from a single hologram with missing central data in multiple reference FTH and HERALDO schemes, respectively. In Fig. 3, an 88×88 pixel object and 2 reference points are embedded into a 512×512 sample mask [Fig. 3(a)]. The holographic condition is satisfied and the exiting wave after the sample mask is generated by assuming a plane wave illumination. The hologram at the far-field plane is calculated as the squared magnitude of the Fourier transform of the exit wave. 41×41 pixels are zeroed out at the center of the hologram to represent the region which is unmeasured due to the BS, as shown in Fig. 3(b). A reconstruction using an inverse FT is shown in Fig. 3(c), which demonstrates severe artifacts. Using our CS method, the object and the twin image are successfully reconstructed without artifacts, as shown in Fig. 3(d).

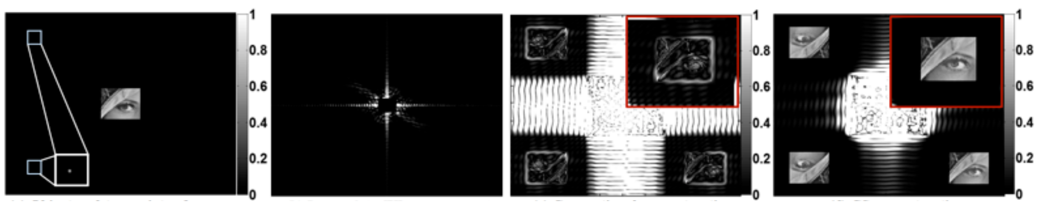


(a) Object and two point references (b) Incomplete FT measurement (c) Conventional reconstruction (d) CS reconstruction

Fig. 3. Image reconstruction from a single hologram with missing central data in multiple references FTH. (a) Sample mask contains an object and 2 references. (b) Simulated hologram with 41×41 pixel region missing in the center. (c) Inverse FT of (b) by setting unmeasured region to zero. (d) CS reconstruction from (b).

HERALDO is a generalization of FTH that uses an extended object as a reference and therefore, increased reference flux. Image reconstruction by HERALDO requires computation of derivatives of the autocorrelation $A_{ff}$ [15-17]. Figure 4(a) shows the same scene as in Fig. 3, but with a thin slit reference object. The simulated hologram (processed as suggested in the reference [15]) with 41×41 pixels missing in the center is shown in Fig. 4(b). The reconstruction, obtained using an IFT, is shown in Fig. 4(c), which has severe artifacts. However, when we apply our CS method, we achieve near perfect reconstruction without losing low-frequency details, as shown in Fig. 4(d). The results displayed in Figs. (3) and (4) clearly demonstrate that the CS method is robust against the missing data problem.

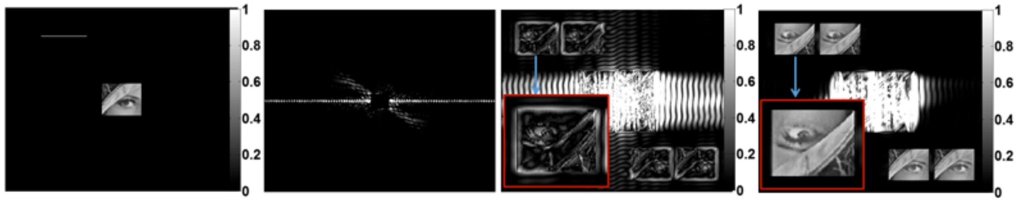

(a) Object and line reference (b) Incomplete FT measurement (c) Conventional reconstruction (d) CS reconstruction

Fig. 4. Image reconstruction from a single hologram with missing central data in HERALDO. (a) The sample mask contains an object and a thin slit reference. (b) Simulated processed hologram with 41×41 pixels region missing in the center. (c) Inverse FT of (b) by setting unmeasured region to zero. (d) CS reconstruction.

To determine how reconstruction quality depends on the amount of missing data and noise, we perform a set of simulations with a "phantom". Reconstructed images from a hologram with varying percentages of missing data are shown in Fig. 5 (left). Signal-to-noise ratio (SNR), defined as $SNR = 10 \cdot \log_{10}\left[\left(\sum S^2\right)/\left(\sum N^2\right)\right]$, where $S$ and $N$ represent the signal and noise, are also calculated to characterize the reconstruction and the measurement on the detector. Note that the intensities behind the beamstop are not included in the measurement SNR calculation. The SNR of CS reconstructions is plotted against sensor noise (Poisson noise) in Fig. 5 (right). From the Fig. 5, it is clear that, for the IFT reconstruction method, SNR degrades significantly even with small amounts of missing data. However, SNR for our CS reconstruction method remains high quality even for large amounts of missing data in the Fourier domain [23].

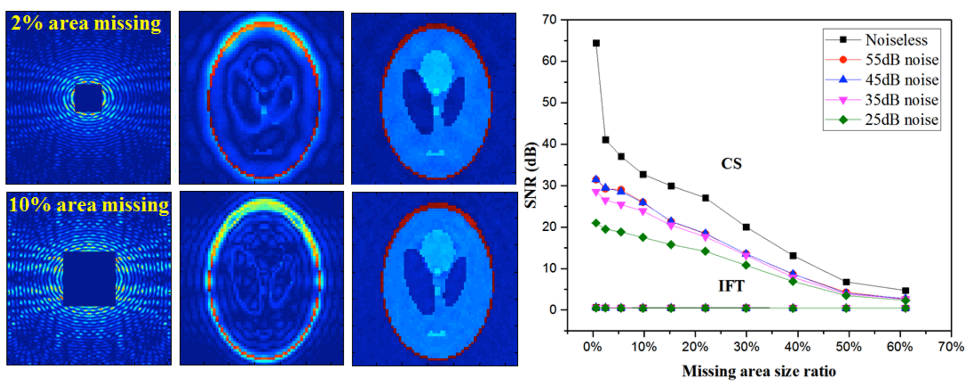


Measurement IFT CS reconstruction

Fig. 5. **Left**: Reconstructed images with different missing area sizes for 35db noise, using IFT and CS algorithms. **Right**: The SNR of reconstructed images is plotted against missing area sizes using IFT and CS methods. Plots for different noise levels are shown in different colors.

*4.3 Experiments on FTH*

We now describe some experimental results illustrating the CS approach applied to FTH. The experimental configuration, shown in Fig. 6.1, is comprised of a collimated laser beam from a laser-diode (532 nm), transmitted through an object mask O. The object mask O is comprised of part of a resolution target of about 1cm×1cm size with a reference point. The reference hole is placed on the top left of the mask, which is about 2.5cm away from the center of the object. The lens L2 (f=300mm) was used to perform a 2D Fourier transform of the object which is collected by a point gray CCD sensor. The measured intensity pattern is shown in Fig. 6.2(a), the red rectangle mimics a beam stop. Figure 6.2(b) shows the direct Fourier transform of the intensity pattern with complete data while Fig. 6.2(c) represents the Fourier transform after removing the central data within the red rectangle, which shows a poor reconstruction. However, CS based reconstruction from the incomplete measurement shows good reconstruction, as shown in Fig. 6.2(d).

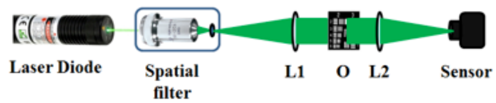


Fig. 6.1. FTH experimental setup. L1: collimator, O: object mask: containing an object and a point reference, L2: Fourier transforming lens.

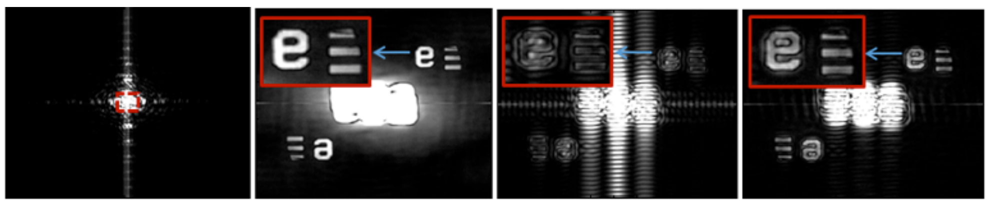

(a) Measurement (b) IFT reconstruction (c) IFT reconstruction from incomplete data (d) CS reconstruction from incomplete data

Fig. 6.2. FTH real experiment. (a) Captured hologram, the red rectangle denotes the missing data area of 41×41 pixels. (b) IFT reconstruction from the complete hologram. (c) IFT reconstruction from incomplete hologram. (d) CS reconstruction from incomplete hologram.

## 5. Coherent Diffraction Imaging (CDI)

*5.1 Description and simulation results*

In CDI, the intensity of the diffraction pattern of an object is measured in the far-field, and then phase is retrieved using iterative algorithms. However, when data in the diffraction pattern is missing due to a beam stop, reconstruction artifacts become apparent and some structural information about the object is permanently lost.

In order to demonstrate the missing data problem with the HIO algorithm [8, 9], we performed simulations with different amounts of missing data. A 128×128 pixel object is embedded into a 512×512 array [Fig. 7(a)]. Figure 7(b) shows simulated diffraction intensity with 512×512 pixels. The central 31×31 pixels in the simulated captured image are removed to mimic effect of a beamstop.

In HIO iterative algorithm, we start with an initial random guess of the object. The following steps are then carried out in the (*k*+1)-th iteration.

1. Compute the Fourier transform (FT) $\hat{G}_{k+1} = F\left\{g_k\right\}$, where $g_k$ is an object reconstruction in the *k*-th iteration.
2. Replace the modulus of $\hat{G}_{k+1}$ with the square root of the diffraction intensities $|G|$. Note that since the intensities are unmeasurable behind the beamstop, the modulus within missing area is kept unchanged. That is,

$$G_{k+1} = \begin{cases} \hat{G}_{k+1}, & \text{for}\left(fx, fy\right) \in B \\ |G| \exp\left(i\phi_{k+1}\right), & \text{for}\left(fx, fy\right) \notin B. \end{cases} \tag{9}$$

where $B$ denotes the beamstop and $\phi_{k+1} = \arg \hat{G}_{k+1}$ is the phase of $\hat{G}_{k+1}$.

3. Calculate the inverse FT of $G_{k+1}$, we have $\hat{g}_{k+1} = F^{-1}\left\{G_{k+1}\right\}$.

4. Update the solution $\hat{g}_{k+1}$ using the HIO method as:

$$g_{k+1} = \begin{cases} \hat{g}_{k+1}, & \text{for}(x, y) \in C \\ g_k - \beta \hat{g}_{k+1}, & \text{for}(x, y) \notin C. \end{cases} \tag{10}$$

where $C$ denotes the object support and $\beta$ is typically selected to be in the interval (0.5, 1) (we used $\beta$ = 0.95). Image reconstruction using the HIO algorithm is shown in Fig. 7(c). Significant artifacts are visible in the reconstructed image.

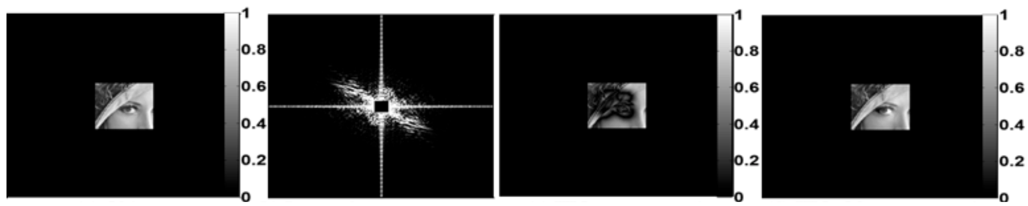


(a) Object (b) Incomplete measurement (c) HIO reconstruction (d) HIO+CS reconstruction

Fig. 7. Reconstruction of a diffraction pattern with missing central data. (a) An original 128×128 pixels image is embedded in a 512×512 pixels array. (b) The diffraction intensity pattern. The data at the central 31×31 pixels are removed. (c) HIO reconstruction after 2000 iterations (d) reconstruction after 2000 iterations using proposed HIO+CS algorithm.

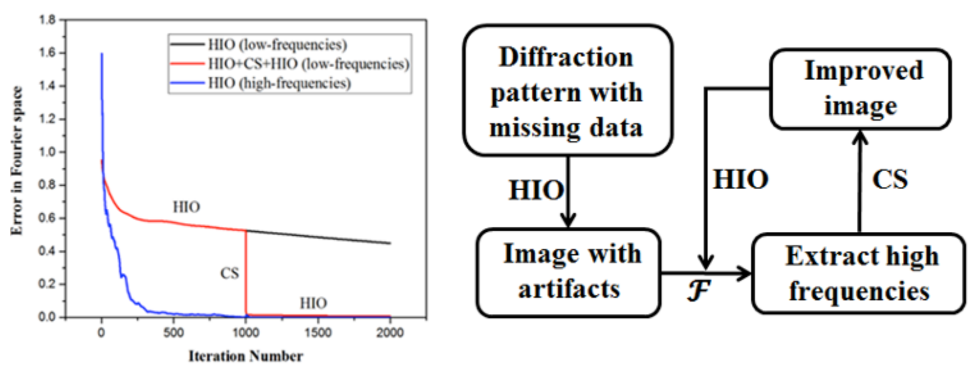


Fig. 8. **Left**: Reconstruction error vs. iteration number of the missing data region (black) and high frequency region (blue) for conventional HIO. Reconstruction error of the missing data region (red) for the proposed HIO+CS algorithm. **Right**: The block diagram of the proposed HIO+CS method.

Figure 8 (left) shows Fourier space RMSE vs. iteration number for the example in Fig. 7. Error is shown for both the central low-frequency region (black) as well as the high-frequencies region (blue). It is clear from the plot that HIO recovers phase accurately in the high frequency region and poorly in the low frequency region. This is because no constraints are provided to force low-frequencies to converge to the correct values. Our approach to solving this problem is as follows: We simply delete the inaccurate low-frequency data from the HIO reconstruction, then apply a CS reconstruction using the accurately recovered phase information from high-frequencies alone. We call this the HIO+CS algorithm. If needed, the reconstruction from HIO+CS can be used as new initial guess for HIO, increasing the convergence of phase retrieval algorithm. The block diagram in Fig. 8 (right) shows how HIO and compressive sensing are combined into a single reconstruction process. The process starts with the incomplete diffraction pattern then goes through several HIO iterations. Because of the missing central data, HIO recovers only high frequency information. In the next step, CS retrieves the lost low frequency information. An optional final step is to again perform several HIO iterations, which may help to improve the result.

The result of applying the HIO+CS algorithm to the simulated diffraction data in Fig. 7(b) is shown in Fig. 7(d). 1000 HIO iterations were first applied, then a single CS step, followed by 1000 more HIO iterations. The low-frequencies in the HIO+CS algorithm approached the true values as shown in the red curve in Fig. 8 (left). Note that in both HIO and HIO+CS reconstructions, we used the same initial seed and same number of iterations. The impact of missing data size and noise (Poisson noise) is shown in Fig. 9. The HIO+CS algorithm is shown to produce high quality reconstructions in comparison to conventional HIO.

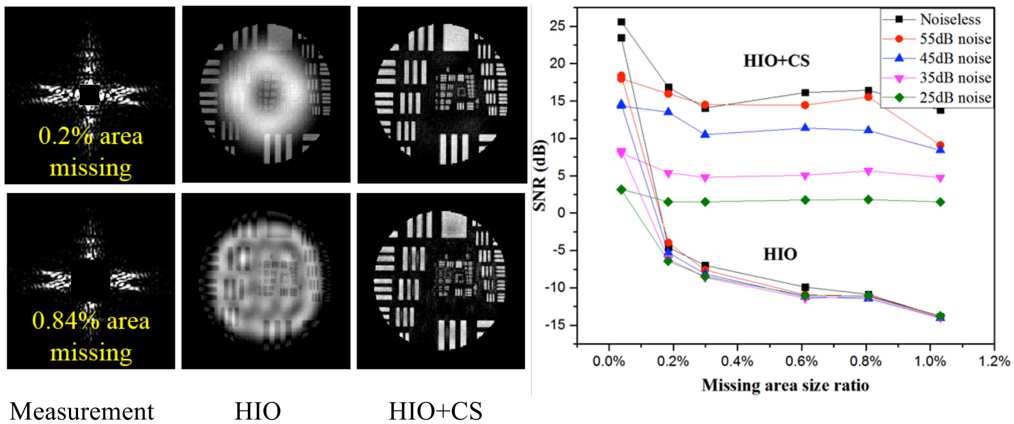


Fig. 9. **Left**: reconstructed images with different missing area sizes using HIO and HIO+CS algorithms (Only central 200×200 pixels are shown out of 512×512). **Right**: The SNR of reconstructed images is plotted against missing area sizes using HIO and HIO+CS algorithms. Plots for different noise levels are shown in different colors.

### *5.2. CDI experiments*

We now describe some experimental results illustrating the HIO+CS approach. The experimental configuration, shown in Fig. 10.1, is essentially same as used for FTH. The only difference is the aperture stop used before the object to apply the aperture constraint in HIO. The object used is a resolution target with aperture support S which is a circular mask of diameter 1.25 cm. The measured intensity pattern is shown in Fig. 10.2(a), the red rectangle mimics a beam stop. Figure 10.2(b) shows the HIO reconstruction with complete data. Figure 10.2(c) shows a HIO reconstruction with missing data after 2000 iterations. Figure 10.2(d) shows an HIO+CS reconstruction, which is considerably better quality than the conventional HIO reconstruction.

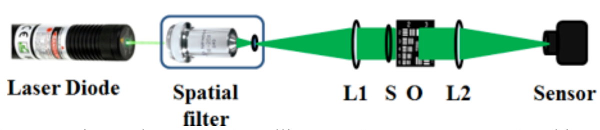


Fig. 10.1. CDI experimental setup. L1: collimator, S: aperture stop, O: object, L2: Fourier transforming lens.

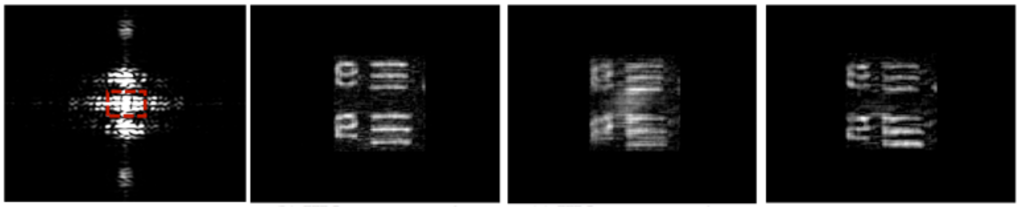

(a) Measurement (b) HIO (complete data) (c) HIO (incomplete data) (d) HIO+CS (incomplete data)

Fig. 10.2. CDI experiment. (a) Captured diffraction pattern with red rectangle showing the removed part. (b) HIO reconstruction after 2000 iterations with complete data (c) HIO reconstruction after 2000 iterations with missing data (d) HIO+CS Reconstruction (2000 HIO iterations total).

## 6. Discussion and conclusions

We have proposed CS-based reconstruction methods to solve the missing data problem in both lensless FTH and CDI by exploiting signal sparsity in a known domain. We showed that CS can be used to accurately recover signals from high-frequencies alone.

For FTH, we analyzed the effects of missing data on reconstruction quality. Conventional FTH reconstructions suffer from (1) artifacts caused by overlap between autocorrelation of the image and the image itself (even when the holographic condition is satisfied) and (2) artifacts due to missing low-frequency information. However, we demonstrated near perfect recovery using our proposed CS-FTH method, even with significant amounts of missing central data in captured holograms. We also demonstrated the accuracy of our technique for multiple reference FTH and extended reference FTH schemes, such as HERALDO.

For CDI, we analyzed the effects of the missing data problem on the HIO reconstruction method. We found, surprisingly, that the error of reconstructed phase is largely contained to within the area of the missing data, while the phase of high-frequencies outside this area is accurately recovered. As a result our HIO+CS based reconstruction algorithm can be used to robustly recover high quality images from CDI data captured with a beam stop.

We believe the work presented in this paper will help to understand the effects of the missing data problem on FTH and CDI techniques. In addition, the CS-based algorithms proposed in this paper will provide a new and efficient way to reconstruct high quality images despite large amounts of missing data in both lensless FTH and CDI regimes. Although we have used amplitude only objects to demonstrate the concept, CS algorithms have been developed for complex objects [37]. Therefore, we expect that our method should also be capable of reconstructing complex objects as well. Our next steps will be to apply our technique to data captured using X-ray synchrotrons (e.g. the Advanced Photon Source at Argonne National Labs). We would also like to theoretically analyze the relationship between the beam stop size and the mutual incoherence of the corresponding high-pass filter matrix. Such a study could give greater intuition into the performance limits of the techniques we propose here.

**Acknowledgments:**
This work was supported in part by NSF CAREER grant IIS-1453192, ONR grant 1(GG010550)//N00014-14-1-0741, and a Northwestern University McCormick Catalyst grant.